Journal of Solid State Chemistry 219 (2014) 49–54

Contents lists available at ScienceDirect

Journal of Solid State Chemistry

journal homepage: www.elsevier.com/locate/jssc

Incorporation of uranium in pyrochlore oxides and pressure-induced phase transitions

F.X. Zhang [a,*], M. Lang [a], C. Tracy [a], R.C. Ewing [a], D.J. Gregg [b], G.R. Lumpkin [b]

[a] Department of Earth and Environmental Sciences, University of Michigan, Ann Arbor, MI 48109, USA
[b] Institute of Materials Engineering, ANSTO, Locked Bag 2001, Kirrawee DC 2232, NSW, Australia

ARTICLE INFO

Article history:
Received 6 May 2014
Received in revised form
7 July 2014
Accepted 9 July 2014
Available online 15 July 2014

Keywords:
Pyrochlore
Uranium
High pressure

ABSTRACT

Uranium-doped gadolinium zirconates with pyrochlore structure were studied at ambient and high-pressure conditions up to 40 GPa. The bonding environment of uranium in the structure was determined by x-ray photoelectron and Raman spectroscopies and x-ray diffraction. The uranium valence for samples prepared in air is mainly U^{6+}, but U^{4+} is present in pyrochlores fabricated in an argon atmosphere. Rietveld refinement of the XRD pattern suggests that uranium ions in pyrochlores are on the 16*d* site in 6-fold coordination with oxygen. At pressures greater than 22 GPa, the pyrochlore structure transformed to a cotunnite-type phase. The cotunnite high-pressure phase transformed to a defect fluorite structure on the release of pressure.

1. Introduction

The pyrochlore structure is a derivative of the ideal fluorite structure [1]. In ordered pyrochlore, there are two distinct cation sites (16*c* and 16*d*) for the cation sublattice with different coordinations to anions on the two anion sites (8*a* and 48*f*). The occupancy of cation species on these sites is mainly determined by their relative sizes. The 16*c* site coordinating with 6 anions on the 48*f* sites and 2 on the 8*a* sites, is usually occupied by larger cations. The 16*d* site is occupied by smaller cations that are coordinated with 6 anions on the 48*f* sites. The structure becomes disordered when *A*- and *B*-site cations are distributed over both the 16*c* and 16*d* sites, as antisite defects. This is most common when the *A*- and *B*-site cations are of comparable size. There is another anion site (8*b*) around the 16*d* site, which is usually empty in ordered pyrochlore. In some cases, anion disordering occurs and oxygens occupy the 8*a*, 8*b* and 48*f* sites. When cations and anions in the structure randomly occupy the corresponding sites in the unit cell, the 16*c*, 16*d* sites and 8*a*, 8*b*, 48*f* sites will become equivalent cation and anion sites, respectively, and the structure becomes a disordered fluorite-type structure with one-eighth of the anions absent. Pyrochlore is thus a $2\times2\times2$ superlattice of the fluorite structure (Fig. 1). The chemical composition of pyrochlore is quite flexible because of the partial occupancy of cations on the 16*c* site and anions on the 8*a* and 8*b* sites [1–5]. Experimental results suggest that the ordered pyrochlore structure forms when $1.46 < r_A/r_B < 1.78$ at ambient conditions [1,6,7], where r_A and r_B are the radii of cations on the *A*- and *B*-site, respectively. The order–disorder transition in pyrochlore can be realized by changing the chemical composition, temperature [1,8,9], exposing to ion irradiation [10–13] and pressure [14–18]. The disordering of cation and anion sublattice in pyrochlore is strongly coherent. Previous experiments reveal that anion disordering may preceed cation disordering in both ion irradiation [12] and high-pressure experiments [14–16] due to the different defect formation energies. However, due to the complexity of the systems, an opposite behavior was also observed [19,20]. The order-disorder transition in pyrochlore can lead to important changes in chemical, electronic and magnetic properties [1]; hence, there is much interest in the disordering process. Proper doping of cations yields larger ionic conductivity that results in pyrochlore oxides that are good ionic conductors with application in the development of solid oxide fuel cells [21–23]. Adjustable energy bands make some of the pyrochlore oxides good catalyst for splitting water [24]. Pyrochlores are also potential candidates for the incorporation of actinides and their disposal in a wide variety of geologic settings [25–28].

Gadolinium zirconate has a cation size ratio of $r_A/r_B = 1.46$, which is on the boundary of the ordered pyrochlore and disordered defect-fluorite structure, and the structure should be sensitive to the doping of actinide elements. An actinide-doped pyrochlore matrix has been reported previously [29–31] and a significant amount of actinide elements can be incorporated into the pyrochlore lattice on both *A*- and *B*-sites [31]. With proper

* Corresponding author.
E-mail address: zhangfx@umich.edu (F.X. Zhang).

http://dx.doi.org/10.1016/j.jssc.2014.07.011
0022-4596/

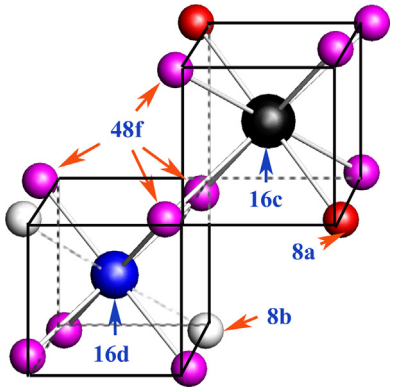

Fig. 1. Local atomic bonding environment of cations in pyrochlore structure. The 16*c* site is eight coordinated with oxygen and 16*d* site is 6-coordinated with six oxygen atoms (48*f*) and the two 8*b* sites are empty.

adjustment of the composition, U^{4+}, U^{5+} and U^{6+} are observed in pyrochlore matrix depending on the conditions of synthesis [30,32].

Previous experiments have revealed that pressure can change the disordering of both the cation and anion sublattices for the pyrochlore structure [14–16]. In addition, the pyrochlore or defect-fluorite structures become unstable at high pressure and transform to a cottunite-type, high-pressure phase [14,15,33]. When the two cations in pyrochlore have a large size difference, the transition pressure is rather high (> 40 GPa for $Gd_2Ti_2O_7$), and the structure becomes amorphous on the release of pressure. For rare earth zirconates with the pyrochlore structure, a pure cotunnite-type high-pressure phase can be obtained at high pressures and the high-pressure phase will transform to a pyrochlore or a defect fluorite-type structure when pressure is released. In this study, we have investigated the behavior of the polyvalent uranium ion and the stability of pyrochlore structure at pressures up to 40 GPa.

2. Experimental method

The uranium-doped pyrochlores were synthesized by a wet chemical method and high temperature treatment. The procedure is described in detail in Ref. [32]. Previous experiments have identified the uranium bonding states in the structure by XRD, electron transmission microscopy, x-ray photoelectron spectroscopy (XPS), diffused reflectance spectrum (DRS) and x-ray absorption near edge structure spectroscopy (XANES). In this study, U-doped pyrochlore with composition of $Gd_{1.8}U_{0.2}Zr_2O_{7+\delta}$ (synthesized in air and argon atmosphere) and $Gd_{1.6}Ca_{0.2}U_{0.2}Zr_2O_{7+\delta}$ synthesized in argon atmosphere were studied by XPS, Raman and synchrotron XRD measurements at ambient and high-pressure conditions. The pressure was generated with a symmetric diamond anvil cell with 300 μm culet size. Hardened stainless steel was indented to around 40 μm thickness which served as gasket. A hole with diameter of 120 μm was drilled on the gasket as the chamber and methanol/ethanol mixture (4/1 in volume) was used as the pressure medium. Pressure was calibrated by using the fluorescence of ruby chips or the diffraction peaks of Au powder [34]. The ambient XRD measurements were conducted at HPCAT, and the high-pressure XRD experiments were conducted at HPCAT and GSECARS at Argonne National Laboratory. The diffraction images were collected with CCD detectors. The Debye rings were integrated into data files with the program Fit 2D [35]. The collected XRD patterns were analyzed using the Rietveld refinement program Fullprof [36]. The oxidation state of U was determined with x-ray photoelectron spectroscopy (XPS) at Kratos Axis Ultra XPS facility in a very high vacuum ($< 10^{-9}$ Torr) environment. UO_2 and UO_3 were used as standards to calibrate the bonding energies of U^{4+} and U^{6+}. The Raman spectra of the samples were measured at ambient and high-pressure conditions with a high resolution Raman spectroscopy (Spex-1250M). A Verdi laser with 532.1 nm wavelength was used as the activation source.

3. Results and discussion

Prior XRD characterization [32] of the synthesized samples confirmed that both samples were a single phase. Fig. 2 shows the XPS spectra of U_{4f} in the pyrochlore together with that of UO_2 and UO_3 as the U^{4+} and U^{6+} standards. The bonding energies of U_{4f} for U^{6+} are a little higher than those of U^{4+}. It is not easy to identify the valence state of uranium in the pyrochlore samples by XPS measurement only. The samples synthesized in air are believed to have the highest valence state because of oxidation. The measured bonding energies in pyrochlore oxides are even a little lower than those of U^{4+} in UO_2. This is due to the differences in bond-length and nearest-neighbor environment. As compared with the sample synthesized in air, the sample synthesized in Ar, $Gd_{1.8}U_{0.2}Zr_2O_7$, has a "tail" in the high-energy region for both U_{4f} 5/2 and U_{4f} 7/2, and the U_{4f} 5/2 and U_{4f} 7/2 peaks are both composed of two peaks. The peaks with lower energy are from U^{4+}, and the peaks with higher energies are from U^{6+}. The sample with the same composition synthesized in air has only peaks close to the high energy peaks, which suggests that U^{6+} is dominant. The XPS measurements indicate that the sample of $Gd_{1.8}U_{0.2}Zr_2O_7$ synthesized in an Ar environment may contain both U^{4+} and U^{6+}, and with the latter as dominant. We cannot identify the U valence states in the pyrochlore sample with composition of $Gd_{1.6}Ca_{0.2}U_{0.2}Zr_2O_7$. The authors in Ref. [32] suggested that it is a mixture of U^{5+} and U^{6+}, but we have no U^{5+} standard for our XPS measurements.

The site occupancy of U ions in the pyrochlore structure is very important. From the high quality synchrotron XRD data, we can complete a quantitative analysis of U-incorporation in the structure at ambient conditions. The expected occupancy of U ions in pyrochlore is on the larger cation size because the uranium ion is larger than that of Zr^{4+}. However, through Rietveld refinement, we found that the occupancy of U in air synthesized $Gd_{1.8}U_{0.2}Zr_2O_7$ is always negative if U is assigned on the 16*c* site. Uranium ions actually share the smaller 16*d* site with Zr^{4+} in 6-fold coordination to oxygen. Also, a portion of the Zr^{4+} (10%) occupies the 16*c* site, and the correct structural formula for this sample is: $(Gd_{1.8}Zr_{0.2})(U_{0.2}Zr_{1.8})O_{7+\delta}$. In order to maintain charge balance, there must be extra oxygen in the anion sublattice if U^{6+} is on the *B*-site. Besides the 8*a* site, another most stable anion site in pyrochlore is the 8*b* site. Rietveld refinement

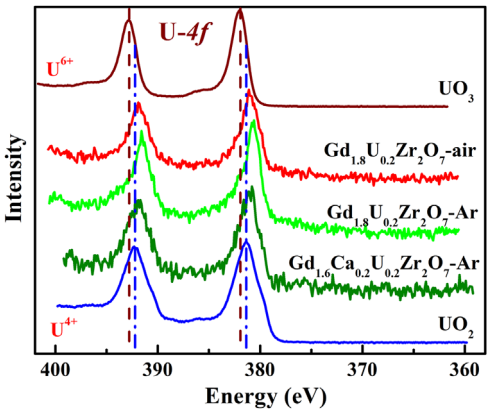

Fig. 2. XPS spectrum of U-doped pyrochlores together with that of UO_2 and UO_3 as the standard of U^{4+} and U^{6+}.

revealed that the correct structural formula of the pyrochlore is: $(Gd_{1.8}Zr_{0.2})(U_{0.2}Zr_{1.8})O_{7.1}$, which maintains the charge balance. The 8*a* site is not fully occupied and a small amount of oxygen (0.31) occupies the 8*b* site. The calculated XRD pattern gives a perfect fit to the observed based on the Rietveld refinement (Fig. 3). For the sample synthesized in argon, the results were similar. For $Gd_{1.6}Ca_{0.2}U_{0.2}Zr_2O_7$ pyrochlore, the U ions also shared the 16*d* site with Zr^{4+}, but the refinement cannot provide insight to the oxygen because of the complicated chemical composition. The refined structural details of $Gd_{1.8}U_{0.2}Zr_2O_7$ synthesized in air are given in Table 1.

The U ion occupancy of the smaller 16*d* site can be rationalized as follows. U^{6+} has a diameter of 0.73 nm and 0.86 nm in 6-fold and 8-fold bonding environment [37], respectively, which is very close to Zr^{4+} in the same environment (0.72 nm and 0.84 nm). Cation disordering in $Gd_2Zr_2O_7$ is expected, and Zr^{4+} occupying the larger 16*c* site has been previously identified by XRD analysis, although Zr^{4+} is smaller than Gd^{3+}.

The Raman spectra of U-doped samples are measured at ambient conditions. Fig. 4 shows the Raman spectra of the samples together with that of undoped pyrochlore sample $Gd_2Zr_2O_7$. $Gd_2Zr_2O_7$ has the pyrochlore structure, but the existence of structural disordering exists and is confirmed by the weak and broad Raman modes and the high fluorescence background. Four Raman active modes were clearly observed in the spectrum. The modes E_g (centered at $\sim$280 cm^{-1}) and A_{1g} ($\sim$520 cm^{-1}) are closely related to the *B* cations and the 48*f* anions around it. The two T_{2g} bands are related to oxygen at the 8*a* site and *A*-site cations. In the U-doped pyrochlores, the change of modes E_g and A_{1g} is more obvious than the change of the two T_{2g} bands, which suggest that the *B*-site cation has changed more in the doped samples, and U ions may mainly share the *B*-site with Zr^{4+}. This is consistent with the Rietveld refinement of the XRD pattern at ambient conditions. The U-doped pyrochlore samples show two distinct Raman active modes with frequencies centered at $\sim$700 cm^{-1} and 740 cm^{-1}, respectively. These two modes are due to the uranium ions in the samples, and two similar modes were found in other uranium oxides, like UO_3 [38], U_3O_8 [39] and U_{60} clusters [40], but with an obvious shift to lower frequencies. In UO_3 and U_3O_8, these two modes are assigned as the stretching modes of O–U–O–U and U–O, respectively. As compared to the samples synthesized in Ar, we can see that the second peak is more identical for the samples synthesized in air. This may be the result of the presence of U^{4+} in the Ar-synthesized samples. U^{4+} has a larger cation radius than that of U^{6+}, and it may prefer to occupy the larger *A*-site in pyrochlore structure. So the site occupancy of U in Ar-synthesized samples may be more complicated.

In order to study the structural stability of U-pyrochlores at high pressure, $(Gd_{0.9}Zr_{0.1})_2(U_{0.1}Zr_{0.9})_2O_{7+\delta}$ (air-synthesized) was investigated up to $\sim$40 GPa. The pressure dependence of the observed XRD patterns is shown in Fig. 5. The pyrochlore structure is stable to 22 GPa, but some extra peaks begin to appear in the pattern at this pressure, which indicates a pressure-induced phase transition. Like pressure-induced phase transitions in other pyrochlores [16], the phase transition in U-pyrochlore is very sluggish. Above 41.8 GPa, a single diffraction pattern of the high-pressure phase is evident. As previously seen, the high-pressure phase is a dense, cotunnite-type phase, but the symmetry may be lower. The normal cotunnite phase is orthorhombic, and there is only one cation site in the structure. The cotunnite-type, high-pressure phase is not stable during release of pressure, and it transforms to a defect fluorite structure gradually, and the quenched sample is nearly a fully disordered fluorite structure (Fig. 5b).

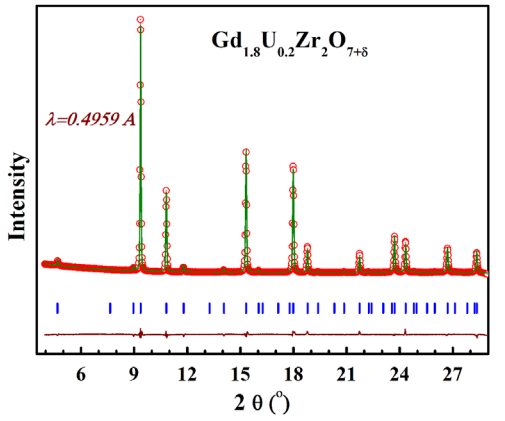

Fig. 3. Rietveld refinement of $Gd_{1.8}U_{0.2}Zr_2O_7$ (air-synthesized) with pyrochlore structural model. The details are listed in Table 1.

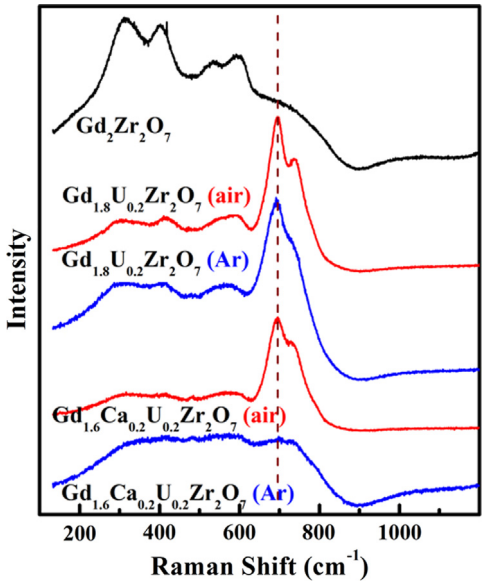

Fig. 4. Raman spectrum of U-doped and undoped $Gd_2Zr_2O_7$ in pyrochlore structure.

Table 1
Crystal structure of $Gd_{1.8}U_{0.2}Zr_2O_7$ (air) pyrochlore as determined by Rietveld refinement. The composition is $(Gd_{0.85}Zr_{0.1})_2(Zr_{0.9}U_{0.1})_2O_{7.1}$, $A=10.5187(3)$ Å.

	A, 16*c* (0,0,0)	*B*, 16*d* (1/2,1/2,1/2)	r_A/r_B	8*a* (1/8, 1/8,1/8)	48*f* (*x*, 1/8,1/8)	8*b* (3/8, 3/8,3/8)
$Gd_{1.8}U_{0.2}Zr_2O_7$	Gd^{3+}/Zr^{4+}	Zr^{4+}/U^{6+}	1.43	0.79(8)	1	0.31(8)
(air)	0.85/0.1	0.9/0.1			0.401(2)	
$Gd_{1.8}U_{0.2}Zr_2O_7$	Gd^{3+}/Zr^{4+}	Zr^{4+}/U^{6+}	1.43	1	1	0
(Ar)	0.82/0.1	0.9/0.1			0.391(1)	
$Gd_{1.6}U_{0.2}Ca_{0.2}Zr_2O_7$	Gd/Ca/Zr	Zr^{4+}/U^{4+}	1.43	1	1	0
(Ar)	0.8/0.1/0.1	0.9/0.1			0.37(2)	

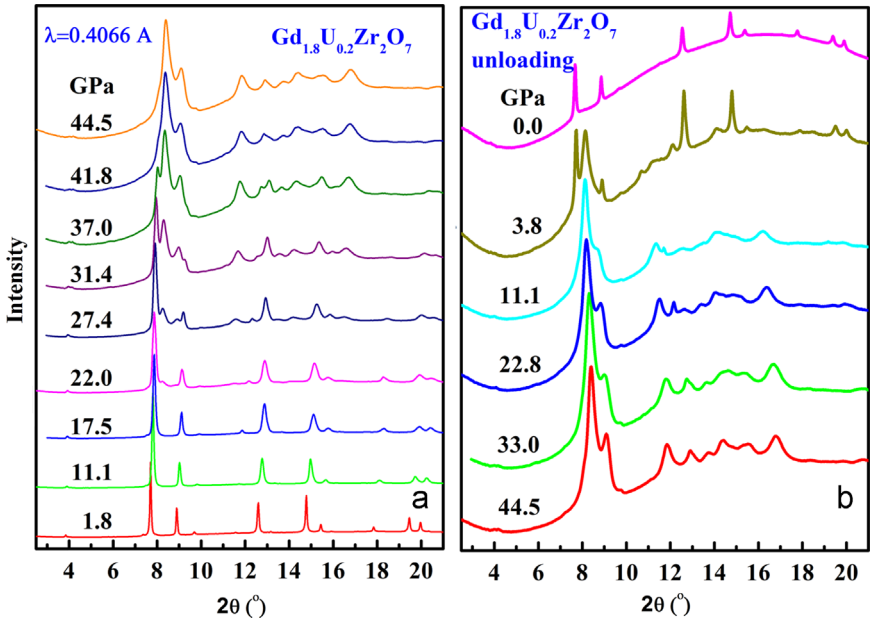

Fig. 5. (a) XRD patterns of air-synthesized $Gd_{1.8}U_{0.2}Zr_2O_7$ at high pressures. A pressure-induced phase transition is obvious at pressure higher than 22 GPa; (b) XRD patterns of air-synthesized $Gd_{1.8}U_{0.2}Zr_2O_7$ during release of pressure.

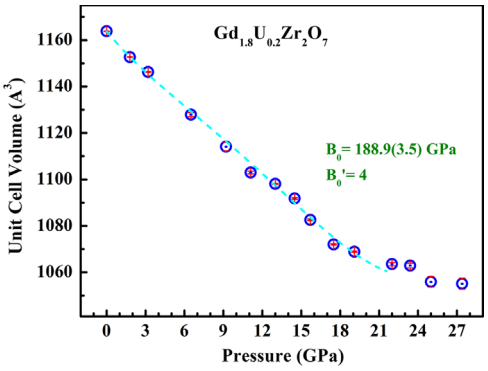

Fig. 6. *P–V* curve of the unit cell volume of air-synthesized $Gd_{1.8}U_{0.2}Zr_2O_7$.

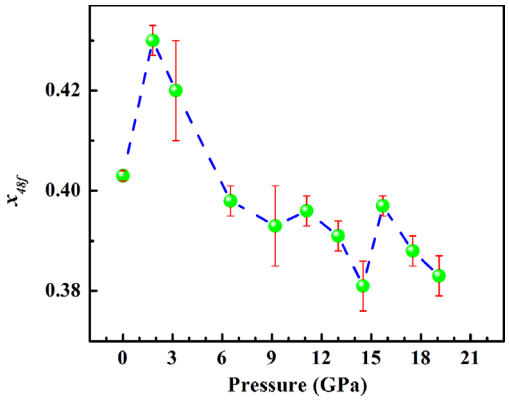

Fig. 7. Pressure dependence of $x48f$ for air-synthesized $Gd_{1.8}U_{0.2}Zr_2O_7$ pyrochlore. Anion disordering occurs mainly below 6 GPa.

The transition pressure of U-doped pyrochlore may be a little higher than that of the undoped $Gd_2Zr_2O_7$ [16], but this effect is not obvious. The unit cell volume of the pyrochlore structure is derived from the refinement of the XRD patterns in the whole pressure range. Fig. 6 shows the pressure dependence of the unit cell volume to high pressures. Fitting the P-V curve of the cubic structure with Birch-Murnagham equation of state yields a bulk modulus of 189 (4) GPa when the first pressure derivative is fixed at $B_0'=4$. This value is compatible with pure $Gd_2Zr_2O_7$ (176 GPa [16]), and doping of uranium in these pyrochlores did not significantly affect the compressibility. The indexing of the diffraction peaks of the high-pressure phase gives the unit cell of the high-pressure phase, and the results indicate that there is around 5% volume collapse during the phase transition.

Previous XRD analysis suggested that disordering in the anion sublattice can be well described with the value of *x*-coordinate of the oxygen at the 48*f* site. The x_{48f} is the only variable atomic coordinate in pyrochlore structure. The fully-ordered pyrochlore structure has an x_{48f} value of more than 0.4, depending on the chemical composition. In the fully-disordered fluorite structure, x_{48f} is 0.375 and the 48*f* site in pyrochlore thus changes to the 8*c* site in the fluorite structure. Through Rietveld refinement of the XRD patterns, the pressure dependence of x_{48f} is plotted in Fig. 7. During pressurization, x_{48f} generally decreases with pressure, which suggests that the anion sublattice becomes disordered with increasing pressure. Pressure-induced anion disordering is more obvious at pressure less than 6 GPa. We cannot provide a precise explanation for the increase of x_{48f} below 2 GPa because of the limited number of data.

The structural evolution of $Gd_{1.8}U_{0.2}Zr_2O_{7+\delta}$ (synthesized in air) was also studied by in situ Raman measurements (Fig. 8). With an increase in pressure, there were no obvious Raman modes detected at pressures higher than 29.2 GPa. XRD results indicate that a cotunnite structure occurs at pressures greater than 22 GPa, but this high-pressure phase may have no detectable Raman active modes due to structural disordering. It is interesting to check the change of U-related Raman active modes in this sample. With increasing pressure, the second peak broadened, and its intensity decrease became obvious. This may be related to the pressure-induced structural disordering. The two peaks may be related to the U cations in the two cation sites in the pyrochlore structure though our XRD results suggest that U mostly occupy the 16*d*-site. At high pressure conditions, the two sites gradually become equivalent, thus, there is only a single peak in the Raman spectrum. At a pressure of 39 GPa, there were no obvious Raman active modes in the whole spectrum range, and only a higher background signal was detected. In order to see the structural changes during release of pressure, the Raman spectrum is shown

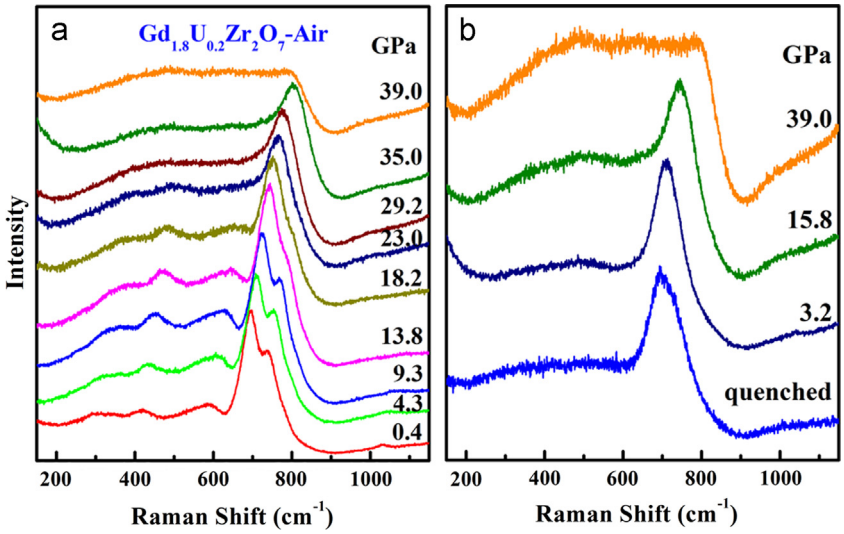

Fig. 8. Pressure dependence of the Raman spectrum of air-synthesized $Gd_{1.8}U_{0.2}Zr_2O_7$ during (a) pressurization and (b) release of pressure.

in Fig. 8b. During release of pressure, the U-related Raman modes have only one peak that has recovered up to 3.2 GPa, which suggests that the recovered sample is still fully disordered during the release of pressure. This is in agreement with the observed XRD patterns during release of pressure. The quenched sample has obviously broad Raman modes, which may contain two active modes, although it is not as clear as the original sample. The XRD pattern of the quenched sample is mainly in fluorite structure, but very weak peak is observable at the lowest two theta angle of 3.8°. This suggests that the recovered sample may contain a minor amount of the ordered pyrochlore structure.

4. Summary

The bonding state of U ions and its occupancy in pyrochlore structure were investigated by XPS, Raman and XRD measurements. The results suggest that U^{6+} is dominant in air-synthesized samples. U^{6+} shares the smaller *B*-site (16*d*) in pyrochlore structure with Zr^{4+}. At pressure greater than 22 GPa, a cotunnite-like high-pressure phase occurs. The doping of U ions in $Gd_2Zr_2O_7$ does not affect significantly the critical transition pressure and compressibility of the pyrochlore structure. The recovered sample was mainly in defect-fluorite structure, which may contain minor amounts of an ordered, pyrochlore phase.

Acknowledgments

This work was supported as part of the Materials Science of Actinides, an Energy Frontier Research Center, funded by the Office of Basic Energy Sciences under Award Number DE-SC0001089. F.Z and M.L also acknowledge the financial support from DOE-NNSA under award number DE-NA0001977. The XRD measurement at GSECARS, Advanced Photon Source (APS), Argonne National Laboratory is supported by the National Science Foundation - Earth Sciences (EAR-0622171), Department of Energy - Geosciences (DE-FG02-94ER14466) and the State of Illinois. The XRD measurements performed at HPCAT (Sector 16), Advanced Photon Source (APS), Argonne National Laboratory are supported by DOE-NNSA under Award No. DE-NA0001974 and DOE-BES under Award No. DE-FG02-99ER45775, with partial instrumentation funding by NSF. Use of the Advanced Photon Source was supported by the U. S. Department of Energy, Office of Science, Office of Basic Energy Sciences, under Contract No. DE-AC02-06CH11357.

References

[1] M.A. Subramanian, G. Aravamudan, G.V. Subba Rao, Prog. Solid State Chem. 15 (1983) 55.
[2] B.J. Wuensch, K.W. Eberman, JOM—J. Miner. Met. Mater 52 (2000) 19.
[3] T. Moriga, A. Yoshiasa, F. Kanamaru, K. Koto, M. Yoshimura, S. Somiya, Solid State Ionics 31 (1989) 319.
[4] J. Wang, A. Nakamura, M. Takeda, Solid State Ionics 164 (2003) 185.
[5] M.P. van Dijk, F.C. Mijlhoff, A.J. Burggraaf, J. Solid State Chem. 62 (1986) 377.
[6] B.C. Chakoumakos, J. Solid State Chem. 53 (1984) 120.
[7] L. Minervini, R.W. Grimes, J. Am. Ceram. Soc. 83 (2000) 1873.
[8] C. Heremans, B.J. Wuensch, J.K. Stalick, E. Prince, J. Solid State Chem. 117 (1995) 108.
[9] A.J. Feighery, J.T.S. Irvine, C. Zheng, J. Solid State Chem. 160 (2001) 302.
[10] R.C. Ewing, W.J. Weber, J. Lian, J. Appl. Phys. 95 (2004) 5949.
[11] K.E. Sickafus, R.W. Grimes, J.A. Valdez, M. Tang, M. Ishimaru, S.M. Corish, C.R. Stanek, B.P. Uberuaga, Nat. Mater. 6 (2007) 217.
[12] S.X. Wang, B.D. Begg, L.M. Wang, R.C. Ewing, W.J. Weber, K.V.G. Kutty, J. Mater. Res 14 (1999) 4470.
[13] J. Lian, X.T. Zu, K.V.G. Kutty, J. Chen, L.M. Wang, R.C. Ewing, Phys. Rev. B: Condens. Matter 66 (2002) 054108.
[14] F.X. Zhang, J.W. Wang, J. Lian, M.K. Lang, U. Becker, R.C. Ewing, Phys. Rev. Lett 100 (2008) 045503.
[15] F.X. Zhang, M. Lang, Z.X. Liu, R.C. Ewing, Phys. Rev. Lett. 105 (2010) 015503.
[16] F.X. Zhang, J. Lian, U. Becker, R.C. Ewing, J.Z. Hu, S. Saxena, Phys. Rev. B: Condens. Matter 76 (2007) 214104.
[17] F.X. Zhang, J. Lian, U. Becker, L.M. Wang, J. Hu, S. Saxena, R.C. Ewing, Chem. Phys. Lett 441 (2007) 216.
[18] F.X. Zhang, B. Manoun, S.K. Saxena, C.S. Zha, Appl. Phys. Lett. 86 (2005) 181906.
[19] S.T. Norberg, S. Hull, S.G. Eriksson, I. Ahmed, F. Kinyanjui, J.J. Biendicho, Chem. Mater 24 (2012) 4294.
[20] Z. Zhang, S.C. Middleburgh, M. de los Reyes, G.R. Lumpkin, B.J. Kennedy, P.E. R. Blanchard, E. Reynolds, L.-Y. Jang, J. Phys. Chem. C 117 (2013) 26740.
[21] P.K. Moon, H.L. Tuller, Solid State Ionics 47 (1988) 28.
[22] H. Yamamura, H. Nishno, K. Kakimuma, K. Nomura, Solid State Ionics 158 (2003) 359.
[23] T. Omata, S. Otsuka-Yao-Matsuo, J. Electrochem. Soc. 148 (2001) E252.
[24] M. Uno, A. Kosuga, M. Okui, K. Horisaka, H. Muta, K. Kurosaki, S. Yamanaka, J. Alloys Compd. 420 (2006) 291.
[25] K.E. Sickafus, L. Minervini, R.W. Grimes, J.A. Valdez, M. Ishimaru, F. Li, K.J. McClellan, T. Hartmann, Science 289 (2000) 748.
[26] A. Chartier, G. Catillon, J.P. Crocombette, Phys. Rev. Lett. 102 (2009) 155503.
[27] W.J. Weber, R.C. Ewing, C.R.A. Catlow, T.D. de la Rubia, L.W. Hobs, C. Kinoshita, H. Matzke, A.T. Motta, M. Nastasi, E.K.H. Salje, E.R. Vance, S.J. Zinkle, J. Mater. Res. 13 (1998) 1434.
[28] K.V. Govindan Kutty, R. Asuvathraman, R. Raja Madhavan, H. Jena, J. Phys. Chem. Solids 66 (2005) 596.
[29] N.K. Kulkarni, S. Sampath, V. Venugopal, J. Nucl. Mater. 281 (2000) 248.
[30] M. James, M.L. Carter, Z. Zhang, Y. Zhang, K.S. Wallwork, M. Avdeev, E.R. Vance, J. Am. Ceram. Soc. 93 (2010) 3464.

[31] B. C. Chakoumakos, Rodney C. Ewing, in: Scientific Basis for Nuclear Waste Management VIII, C. M. Jantzen, J. A. Stone and Rodney C. Ewing, (Eds.), MRS Proceedings, vol. 44, Pittsburgh, Pennsylvania, 641-646 (1985).
[32] D.J. Gregg, Y Zhang, Z. Zhang, I Karatchevseva, M.G. Blackford, G. Triani, G.R. Lumpkin, E.R. Vance, J. Nucl. Mater. 438 (2013) 144.
[33] F.X. Zhang, M. Lang, U. Becker, R.C. Ewing, J. Lian, Appl. Phys. Lett. 92 (2008) 011909.
[34] Y. Fei, J. Li, K. Hirose, W. Minarik, J.V. orman, C. Sanloup, W. van Westrenen, T. Komabayashi, K. Funakoshi, Phys. Earth Planet. Inter. 143-144 (2004) 515.
[35] A. Hammersley, Computer Program Fit 2d (ESRF, Grenoble, 1998).
[36] T. Roisnel, J. Rodriguez-Carvajal, Mat. Sci. Forum, in: Proc. Seventh Eur. Powder Diffr. Conf. (EPDIC7), 118 2000.
[37] R.D. Shannon, Acta Crystallogr., Sect. A: Found. Crystallogr. 32 (1976) 751.
[38] M.L. Palacios, S.H. Taylor, Appl. Spectrosc. 54 (2000) 1372.
[39] D. Manara, B. Remker, J. Nucl. Mater. 321 (2003) 233.
[40] B.T. McGrail, G.E. Sigmon, L.J. Jouffret, C.R. Andrews, P. Burns, Inorg. Chem. 53 (2014) 1562.